IEEE JOURNAL OF
SELECTED TOPICS IN QUANTUM ELECTRONICS
A PUBLICATION OF THE IEEE PHOTONICS SOCIETY
IEEE photonics Society
SEPTEMBER/OCTOBER 2015 VOLUME 21 NUMBER 5 IJSQEN (ISSN 1077-260X)
ISSUE ON ATTOSECOND PHOTONICS

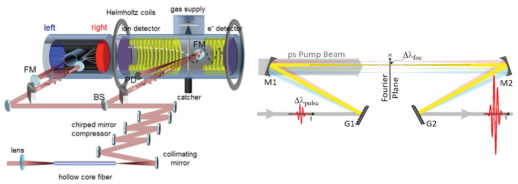

(Left) Schematic of the experimental setup consisting of a single-shot Stereo-ATI phase meter (left chamber) and a reaction microscope (REMI) spectrometer (right chamber). A beam splitter (BS) and focusing mirrors (FM) direct the laser pulses into both chambers. Each arm is equipped with a pair of fused-silica wedges for compensating residual chirp. In the Stereo-ATI, xenon atoms are ionized near the focus of the horizontally polarized laser beam, and the electrons produced are detected by microchannel-plate (MCP) detectors to the left and to the right, enabling the determination of the CEP for each REMI event. (B. Bergues *et al.*, article number 8701009)
(Right) The frequency domain OPA (FOPA) setup rests upon a *4f* configuration which maps the spectral content of an incident few-cycle pulse onto a spatial coordinate in the Fourier plane. There, the seed beam is intrinsically stretched to ps duration and can interact with a ps pump beam. Separate stretcher and compressor are not required. Different, individually tunable crystals may be employed in the Fourier plane. Thus, by increasing the number of crystals, the FOPA output properties are not limited by the performance of a single crystal. (P. Lassonde *et al.*, article number 8700410)

This article was published in:

K. Kovács, V. Toa, B. Major, E. Balogh and K. Varjú, "High-Efficiency Single Attosecond Pulse Generation With a Long-Wavelength Pulse Assisted by a Weak Near-Infrared Pulse," in IEEE Journal of Selected Topics in Quantum Electronics, vol. 21, no. 5, pp. 1-7, Sept.-Oct. 2015.
DOI: 10.1109/JSTQE.2015.2411580

Available online at:
http://ieeexplore.ieee.org/document/7056492/

High efficiency single attosecond pulse generation with a long wavelength pulse assisted by a weak near infrared pulse

Katalin Kovács, Balázs Major, Emeric Balogh, Valer Tosa, and Katalin Varjú

***Abstract*—We model two-color high-order harmonic generation using a full 3D non-adiabatic model and show that the presence of a weak perturbative near infrared pulse assisting a strong pulse of long wavelength increases the high-harmonic yield with one order of magnitude in the whole spectral range up to 160 eV. In addition we demonstrate that it is possible to obtain a single attosecond pulse at the exit of the interaction region even by starting from two laser pulses of 50 fs each.**

***Index Terms*—high-order harmonic generation, 3D simulation, single attosecond pulse, phase-matching, trajectory analysis.**

I. Introduction

RECENTLY, due to the availability of powerful OPA systems, strong laser pulses in the mid-IR (MIR) spectral domain can be produced in many laboratories [1]–[4]. For high–order harmonic generation (HHG) this is an important achievement because it is known that the cutoff frequency at single–dipole level is governed by the $E_{\mathrm{cutoff}} = I_p + 3.17\frac{e^2E^2}{4m\omega^2}$ law, therefore strong MIR pulses would be advantageous to be used as fundamental pulses in HHG compared to the mostly used near-infrared (NIR) 800 nm pulses. However, the conversion efficiency of the HHG process drops as $\sim \lambda^{-5} - \lambda^{-6.5}$ [5], [6], and this is the reason why different techniques have been developed to increase HHG efficiency.

Most of the proposed methods to enhance the yield of HHG rely on the increase of the number of emitters. This can be achieved by expanding the interaction volume using a loose focusing geometry [7]–[11], applying a laser beam with flat-top profile [12], or by quasi phase-matching. Quasi-phase-matching has already been achieved in periodic gas jets [13], in modulated hollow-core waveguides [14]–[16], or by employing a counter- or perpendicularly propagating weak assisting pulse [17]–[19]

Naturally, increasing the cut-off of the high-harmonic spectrum without too high loss of yield is also an important problem to solve. Considering the source of the radiation, an obvious way is to use ionized medium to exploit its higher ionization potential using a capillary discharge [22]. Apart from the evident approach to use longer wavelength drivers [2]–[4], a prevailing solution for cut-off extension is to combine the generating NIR/MIR beam with another one (or several others) of different wavelengths [24]–[30]. This latter is generally named as two-color HHG, and has the advantage of high tunability as the polarization [25], [28], the relative phase [24] and the wavelengths of the two pulses can be set, and this technique can also be combined with other methods of yield enhancement and single attosecond pulse (SAP) generation [8], [26].

In this paper we propose a novel version of the two–color HHG configuration, in which a strong MIR pulse plays the role of the driving pulse and is assisted by a much weaker NIR pulse. We present here the details of the gating effect due to the presence of the assisting NIR pulse: we begin by exploring the NIR influence from the single–dipole level at optical half–cycle temporal resolution, and proceed by presenting the macroscopic effects that arise during the propagation of the two pulses in the ionized gas medium. We discuss the main effects due to the presence of the weak NIR pulse, i.e. the modified temporal separation between successive emissions, trajectory shortening, modified ionization dynamics and driving pulse distortions, dominance of the off–axis contribution to the final harmonic power spectrum, and the gating mechanism leading to single attosecond pulse production.

II. Modeling tools and input parameters

We use a 3D non-adiabatic model first described in [31] which was extended [32] to be able to handle the two-color configuration for both the propagation of the fundamental pulses and the HHG. The simulation closely follows the real physical processes, and has three main steps: (1) the driving pulses are propagated through the medium by solving the wave equation

$$\nabla^2\vec{E}(r,z,t) - \frac{1}{c^2}\frac{\partial^2\vec{E}(r,z,t)}{\partial t^2} = \frac{\omega_0^2}{c^2}\left(1-\eta_{\mathrm{eff}}^2\right)\vec{E}(r,z,t) \quad (1)$$

This is written in a frame moving with the pulse, it is discretized using the Crank–Nicholson scheme and solved in the Fourier space using the paraxial approximation and assuming cylindrical symmetry. The laser fields may ionize the noble gas medium and they propagate in the plasma created by their joint action. The space- and time-dependent effective refractive index $\eta_{\mathrm{eff}}(r,z,t)$ includes the dispersion of neutral atoms, the optical Kerr–effect and plasma dispersion. In step (2) the single–dipole response of the medium is calculated using the strong field approximation **(SFA)** [33]. The nonlinear

K. Kovács is with the National Institute for Research and Development of Isotopic and Molecular Technologies, 400293 – Cluj-Napoca, Romania and also with ELI-ALPS, ELI-Hu Nkft, Dugonics tér 13, Szeged 6720, Hungary

B. Major, E. Balogh and K. Varjú are with the Department of Optics and Quantum Electronics, University of Szeged, 6720 Szeged, Hungary

V. Tosa is with the National Institute for Research and Development of Isotopic and Molecular Technologies, 400293 – Cluj-Napoca, Romania

Manuscript received .....; revised .....

polarization of the medium is calculated from the single-atom time-dependent dipole moment, that is obtained by solving the Lewenstein integral:

$$x_{\mathbf{n}}(t) = i\int_0^t dt' \int d\mathbf{p}\ \mathbf{n}\cdot\mathbf{d}^*(\mathbf{p}+\mathbf{A}(t))\exp[-iS(\mathbf{p},t,t')] \\ \mathbf{E}(t')\cdot\mathbf{d}(\mathbf{p}+\mathbf{A}(t')) + c.c. \quad (2)$$

where $\mathbf{n}$ **is the direction of the dipole**, $\mathbf{A}$ denotes the vector potential of the laser pulse, $\mathbf{d}$ the dipole matrix element for the bound–free transition, and $S(\mathbf{p},t,t')$ the quasiclassical action. Finally, in step (3) the harmonic field is propagated until the detection point by solving the same wave equation as in (1), but with the source term being the non–linear polarization of the medium as calculated in (2). The dispersion and absorption of the harmonics are taken into account.

To gain further insight to the process, the electron trajectories are calculated using a method based on the solution of the saddle–point equations with complex–valued variables [34]:

$$\frac{\alpha(t_b)-\alpha(t_r)}{t_r-t_b} = \mathbf{p}_s \quad (3)$$

$$[\mathbf{p}_s+\mathbf{A}(t_b)]^2 = 2I_p \quad (4)$$

$$[\mathbf{p}_s+\mathbf{A}(t_r)]^2 = 2(q\omega+I_p), \quad (5)$$

where $\alpha(t) = \int^t \mathbf{A}(t'')dt''$ and $\mathbf{p}_s$ is the canonical momentum. This method has been integrated into the main 3D non-adiabatic model and facilitates the control of the whole HHG process at optical half-cycle level by giving direct information about the trajectories of interest: ionization (t_b) and recollision times (t_r), canonical momentum ($\mathbf{p}_s$) and trajectory phase. The phase accumulated by an electron trajectory which generates harmonic order q at a specific burst k in time during the laser pulse is calculated with equation:

$$\phi_q^{(k)} = \mathrm{Re}\left[q\omega_0 t_r^{(k)} - \int_{t_b^{(k)}}^{t_r^{(k)}}\left(\frac{[\mathbf{p_s}+\mathbf{A}(t)]^2}{2} - I_p\right)dt\right]. \quad (6)$$

Our intention is to perform simulations with pulses that can be routinely obtained in laboratories, and we demonstrate that even with long pulses it is possible to obtain both extended cutoff and high photon yield. Additionally, we show that SAP can also be obtained by filtering the cutoff region and the detector placed in the far–field.

In the simulations we carefully selected parameters that are available or feasible in HHG laboratories. The main input parameters are the following: primary pulse (MIR): $\lambda_{\mathrm{MIR}} = 1300$ nm, $E_{MIR} = 2.6$ **mJ**, $I_{\mathrm{peak}} = 9\cdot10^{14}$ W/cm^2 (in the focus in vacuum), $\tau_{\mathrm{FWHM}} = 50$ fs; secondary pulse (NIR): $\lambda_{\mathrm{NIR}} = 790$ nm, $E_{NIR} = 0.25$ **mJ**, $I_{\mathrm{peak}} = 1\cdot10^{14}$ W/cm^2 (in the focus in vacuum), $\tau_{\mathrm{FWHM}} = 50$ fs. Both pulses are Gaussian in time and space (at the entrance of the HHG cell), linearly polarized, parallel to each other and propagate in the same direction. The time delay between the two pulses is kept zero and both pulses are focused with a $f = 50$ cm mirror into a 6 mm long static cell filled with 500 mbar Ne. The interaction region is placed 10 mm upstream the laser focus, because it has been shown [35], [36] that in the high–pressure and high ionization conditions it is advantageous to place the cell before focus. At this position the peak intensity of the primary (MIR) driving pulse when entering the cell is $3.7\cdot10^{14}$ W/cm^2 and the beam radius is 92 μm. Similarly, the peak intensity of the secondary (NIR) pulse is $0.6\cdot10^{14}$ W/cm^2 at cell entrance. The role of the parameter choice will also be discussed in the next section, with special attention paid to the beneficial role of the longer then usual gas cell. The focusing and generation medium conditions employed in this particular case study were inspired by the real experimental conditions used in a series of experiments at MBI Berlin. **In Fig. 1 (a) we schematically represent the geometrical arrangement of the studied configuration. The beams propagate from left to right along z axis, $z = 0$ in the focus. In Fig. 1 (b) and (c) we show the MIR and NIR pulses at the entrance and at the end of the HHG cell, respectively. The reasons and consequences of the strong pulse distortion will be discussed in sections III-D and III-E.**

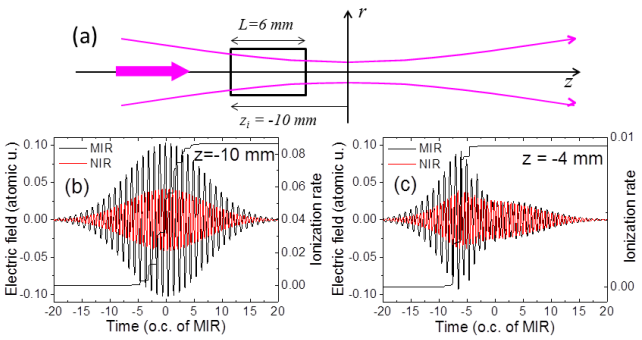

Fig. 1. (a) Schematic reprezentation of the HHG geometry. (b) MIR and NIR pulse shapes at the entrance in the GGH cell, i.e. at z=-10 mm. (c) MIR and NIR pulse shapes after propagation through the 6 mm long gas cell, i.e. at z=-4 mm.

III. Results and Discussion

A. HHG spectra: cutoff and yield

Throughout the paper harmonic yields and power spectra are given in arbitrary units as given by the SFA Lewenstein integral. However, the results obtained in different HHG configurations are directly comparable and allow a relative measure of the harmonic efficiency. We show typical near–field HHG spectra at the end of the medium in Fig. 2. By adding a very weak NIR pulse to the main MIR, the HHG spectrum changes drastically: the MIR-only cutoff was at 200 eV, while the two-color spectrum's cutoff is reduced to 160 eV. On the other hand, the efficiency of the two-color HHG is increased by an order of magnitude compared to the MIR-only spectrum in the whole spectral range up to the two-color cutoff. We note that the NIR pulse alone does not produce harmonics in this spectral range, so its effect is solely assisting the MIR harmonic generation.

In the following we explore the mechanisms that cause cutoff reduction and yield enhancement when a very weak NIR pulse assists the HHG process. In addition we will examine the conditions for obtaining SAP in this configuration.

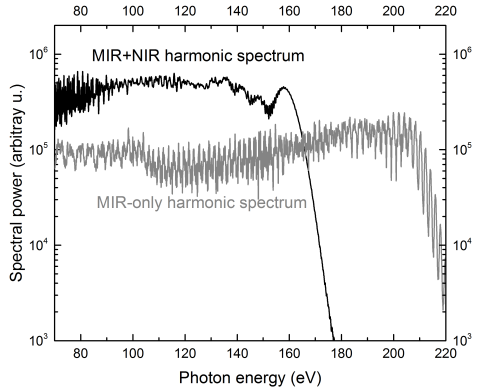

Fig. 2. Simulated near–field HH spectra at the exit of the cell. Gray: spectrum generated with the MIR pulse only. Black: HH spectrum obtained with combined MIR+NIR pulses. Laser parameters and generation conditions are in the main text.

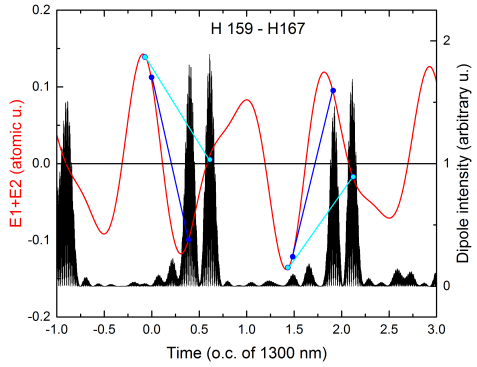

Fig. 3. The presence of a perturbative NIR pulse changes the half-cycle symmetry of elementary high-harmonic dipole emissions. Central part of the combined pulse shape is shown with the dipole emissions filtered between H159 and H167. The lines with dots at the ends describe the electron trajectories in the Kramers-Henneberger frame.

B. Single–dipole generated in a two–color field

It is already visible in Fig. 2 that the two-color spectrum has denser line structure. This is due to the fact that the presence of an assisting NIR pulse alters the half–cycle symmetry of the MIR field. In Fig. 3 we show the single–dipole response of the medium in the combined field. The elementary bursts occur with a periodicity of 1.5 o.c. of the driving MIR pulse, which corresponds to an "effective wavelength" which is the least common multiple of the 790 nm and 1300 nm, i.e. approximately 3900 nm. As seen in Fig. 3 a very weak NIR pulse is sufficient to induce the large temporal spacing of successive dipole emissions.

To understand the cutoff mechanism in this particular two–color field we look in more detail at the harmonic signal in the ≈150-160 eV spectral range, corresponding to harmonics from order 159 (H159) to 167 (H167). The time-dependent emission of this field at the entrance in the medium is shown in Fig. 3. At the beginning of the interaction region the two laser pulses are unperturbed, and this spectral range belongs to the plateau region, therefore the short and long trajectory components are well separated. Performing the trajectory analysis for H159 at different positions in the cell, and comparing the durations

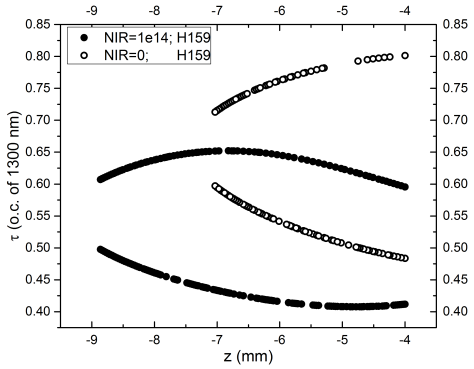

Fig. 4. Trajectory shortening due to a small perturbative NIR field. Open circles: short and long trajectories produced by the MIR pulse alone. Filled circles: trajectories contributing to the same harmonic burst produced in the MIR+NIR case. The trajectories correspond to burst at -6 o.c., H159, on–axis evolution.

of the trajectories ($\tau = t_r - t_b$) contributing to the same harmonic burst in the absence and in the presence of the assisting NIR pulse, we see a clear trajectory shortening caused by the weak NIR (Fig. 4). The released electrons spend shorter time in the continuum in the two–color field, therefore they are less exposed to wave-packet spreading. Since the main disadvantage of using MIR as driving pulse for HHG is the serious wave-packet spreading, the trajectory shortening will reduce this disadvantage and contribute to the relatively increased HHG efficiency. We consider that the increased efficiency in the present case has also macroscopic contributions, i.e. due to propagation effects, as we will see in the following.

C. Role of NIR field during propagation

The intensity of the assisting NIR pulse is low compared to the MIR pulse intensity, however, it strongly influences the ionization mechanism throughout the propagation. At the beginning of the interaction region the ionization level is 8% for the two–color case, while only 0.8% in the MIR–only case. After 6 mm of propagation in 500 mbar Ne the ionization fractions are 0.9% and 0.8% respectively. We emphasize here that even less then 1% ionization fraction causes a non–negligible electron density because of the high gas pressure [35], therefore the conditions for HHG cannot be considered being (close to) neutral. In fact an ionization rate of 0.8% lays between the critical phase-matching ionization rates for the 1300 nm (0.4%) and 800 nm (1%) driver pulses [37].

Fig. 5 shows the evolution of the MIR peak intensity during propagation alone (a) and in the presence of the weak NIR pulse (b). In the latter case the MIR is exposed to stronger distortion: although the interaction region is before the laser focus the pulse intensity decreases, but reaches an almost constant effective intensity which is maintained in the second half of the gas cell and extends also in radial direction for about 50 μm. The reduced MIR intensity in the two–color configuration is the reason for the reduced cutoff seen in Fig. 2. Indeed for $4 \cdot 10^{14}\,\mathrm{W/cm^2}$ peak intensity the single–atom cutoff is at 220 eV, while for $3 \cdot 10^{14}\,\mathrm{W/cm^2}$ it is at 170

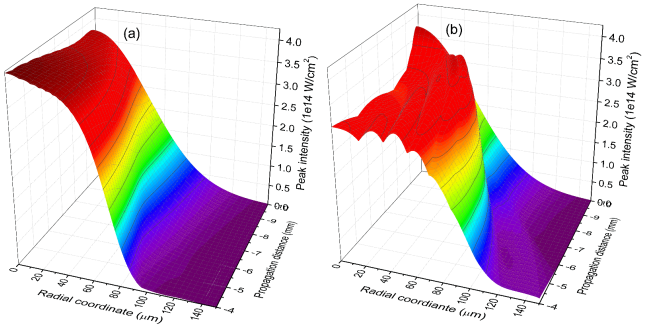

Fig. 5. Evolution of the primary MIR pulse peak intensity along propagation. (a) MIR propagates alone. (b) MIR pulse is assisted by the weak NIR pulse.

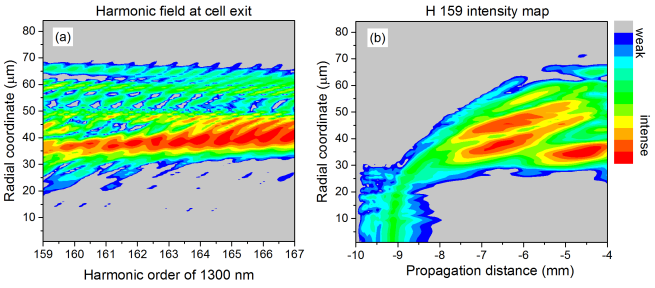

Fig. 6. (a) Radial structure of the harmonic range between H159–H167 recorded at the exit of the interaction region. (b) Selected harmonic order H159 map as it builds up during propagation. The scale for both color maps is logarithmic, covers two orders of magnitudes, the units are arbitrary.

eV, values which are comparable with the cutoffs seen in the near–field spectra in Fig. 2. Propagated laser (Fig. 5 (b)) and harmonic (Fig. 6) field intensities exhibit a clear correlation between their spatial structures. In particular we note that, unlike the usual one-color case, the cutoff harmonics are formed off–axis, where the total laser intensity is higher than on–axis and the phase–matching conditions seem to facilitate the coherent construction of the cutoff harmonics. The off-axis generation also increases the effective gas volume, hence it also contributes to the increased generation efficiency shown in Fig. 2.

D. Harmonic field build–up

We examine now the circumstances of how the strong harmonic radiation in the cutoff region is formed. In Fig. 6 (a) we show the (ω, r) map of the harmonic field intensity at the exit of the medium. It is clear that the main contribution to the spectral power comes from off–axis harmonic radiation, as we already anticipated in the preceding section. Selecting one harmonic order (H159) we can follow the construction of this harmonic along the medium, and this is shown in Fig. 6 (b). This harmonic order meets favorable phase–matching conditions in a band at $\approx 30 - 50\mu$m off–axis. It is also shown in Fig. 6 (b) that the field sources (the oscillating single dipoles) build-up constructively only in the second half of the medium, so that at the exit an intense XUV radiation can be detected. The region where the H159–H167 spectral domain is amplified coincides with the region of slow intensity variation of the driving MIR pulse in z direction, see Fig. 5 (b).

Since the two laser fields are multi–cycle pulses, it is expected that at dipole level there are multiple emissions within the combined pulse, as seen in Fig. 3. In the 3D model there is the possibility to follow the harmonic build–up also in time in the reference frame moving together with the generating pulses. In Fig. 7 we show the evolution of the single–atom dipole emissions (top row) throughout the generation cell, along with the propagated harmonic field (bottom row) as it is constructed from the coherent superposition of successive dipole emissions. **As we observe, significant dipole emission is in the leading edge of the main MIR pulse. Comparing Figures 7. and 1. we see that the pulses suffer serious reshaping and the rising edge will be responsible for HHG.** Following the process of coherent build–up of the harmonic radiation we can see that the successive emissions find favorable phase–matching conditions in just one single half cycle, this is at -4 o.c. in the leading edge of the main MIR pulse. The first remark here is that this particular time–window within the pulse becomes ”active” only in the second half of the gas cell. In fact this burst is built mainly from the high intensity harmonic field seen at around 35–40 μm in Fig. 6 (a) which develops also in the second half of the medium, as evident in Fig. 6 (b) for H159. The second thing to remark is the big difference between the dipole emissions and the propagated harmonic field, especially on-axis. Indeed, the on–axis emission seen in the dipole in the earlier cycles (from -7 to -4 o.c.), do not find favorable phase-matching conditions during propagation and fail to build up to a strong coherent XUV radiation. This is due mainly to the higher dispersion induced on-axis by the rapid variation of the intensity and hence ionization level (see in Fig. 5 (b) the drop of the initial intensity), and is a clear example in which propagation effects are dominant in the HHG process. On the other hand this is also an example of how propagation can help to obtain SAP by weakening all emissions but one.

The trajectory analysis offers a zoom into the details of the harmonic burst construction process. We try to answer the question: what properties make the off–axis radiation at -4 o.c. to survive and become the strongest in intensity in near–field? In Fig. 8 (a) we present the durations of the electron trajectories that recombine with the parent atom around -4 o.c. and which contribute to H159. We also present in Fig. 8 (b) the corresponding phase variation of the trajectories. It is worth to note that these trajectories appear only in the last third of the medium, which extends from -6 to -4 mm (the cell begins at -10 mm). One can immediately note that these trajectories, especially the shorter one, have small phase variation as propagation proceeds, therefore their contributions to the burst at -4 o.c. will interfere constructively yielding a strong harmonic emission at the medium exit. As a comparison, we examined the phases of the trajectories generating the burst at -6 o.c. on–axis at the same order H159 (see their durations in Fig. 4) and saw that in the same propagation domain (from -6 to -4 mm) these phases vary 20–40 radians. It is thus expected that at -6 o.c. on–axis there is no strong XUV pulse detectable at the end of the HHG cell,

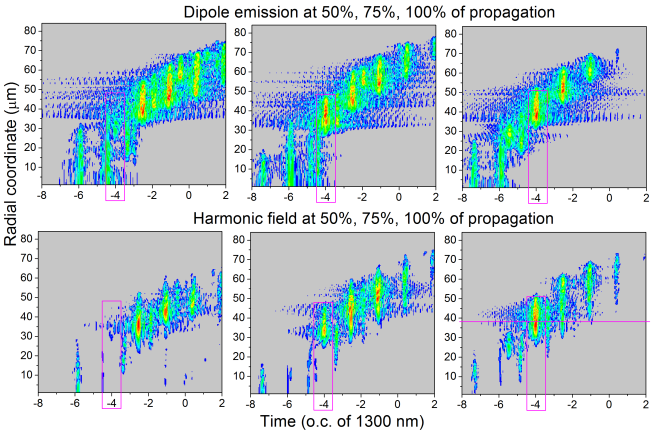

Fig. 7. Top row: Radial structure of the dipole emissions in the H159–H167 spectral range as they are emitted in the relevant part of the driving pulse. At three particular positions during pulse propagation in the HHG cell these (t,r) maps are presented (from left to right): at 50%, 75% and 100% of the cell. Bottom row: the same structure as above presented for the propagated harmonic field. The scale for all color maps is logarithmic, covers two orders of magnitudes, the units are arbitrary, but the same within one row. The rectangular windows follow the evolution of the burst which at exit will be the highest in intensity. The time is plotted in optical cycle units of the 1300 nm field (4.33 fs) with zero time at the pulse center.

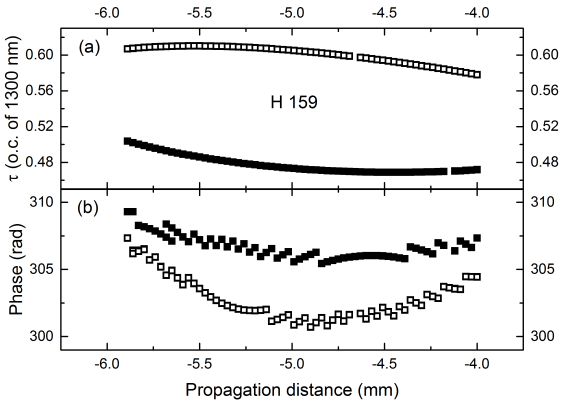

Fig. 8. Trajectory analysis for H159 of the strongest burst at -4 o.c. at 40 μm from the optical axis as indicated by the horizontal line in Fig. 7. (a) Trajectory duration as a function of propagation distance. (b) The trajectory phases as propagation evolves. Same symbols stand for the same trajectories.

as can be followed on the panels in Fig. 7.

E. Single attosecond pulse

We are interested in SAP features not only in the near–field but also after the XUV radiation leaves the interaction region, in the far–field. This is why we examine here the XUV near and far fields in the spectral range around the cutoff, i.e. 150–160 eV. In Fig. 9 we present the radially integrated harmonic field as it is detected in time domain: black is in the near–field just at the medium exit, while the gray curve shows the signal detected in the far–field. In our calculation we assume that the XUV radiation is detected 1.2 m downstream the HHG cell after it passes through and iris of 10 mm diameter placed in the far field.

As one can see from Fig. 9 the near–field harmonic emission has one main attosecond pulse followed by two satellites.

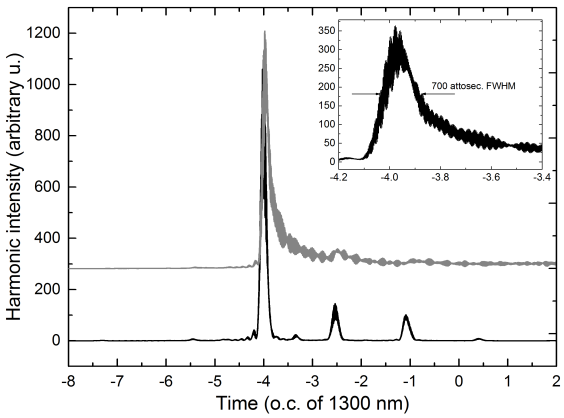

Fig. 9. Attosecond pulses synthesized from 150-160 eV radiation. Black line: near–field harmonic signal integrated radially. Gray line: far–field harmonic signal integrated radially, shifted up for better viewing. Inset: zoom into the SAP in the far–field, its duration is 700 attoseconds.

The strongest pulse corresponds to the radiation at -4 o.c. which is generated at 35–40 μm away from the optical axis, as seen in Fig. 7, while the two following bursts come from the successive emissions which are farther off–axis and much weaker. The intensity ratio of the strongest and the second strongest pulses is 7.6 : 1. This is not an exceptional contrast, but we note that these pulses are separated by 6.5 fs. This large time delay might be exploited in pump-probe experiments, or temporally filtering the satellites the strongest SAP could be used in the desired applications. The main attosecond burst's duration is 530 attosec FWHM and has a remarkably good contrast. This is due to the fact that all the contributions to this burst are emitted in a narrow time window for several micrometers in radial direction (see Fig. 7). **The spectral filter for SAP is in the cutoff spectral region, yet we can identify two sets of contributing trajectories with comparable time spent in the continuum as seen in Fig. 8. Analyzing their recombination times we found that the cut-off "shorter" trajectories recombine at slightly earlier times and give the sharp leading edge and peak of the SAP in Fig. 9., while the cut-off "longer" components give the trailing edge of the SAP.**

Looking at the temporal structure in the far–field, we see a clear SAP with the same high contrast in the leading edge as in the near–field. However, this time the two satellite pulses are no longer present in the far–field. This is due to the iris placed in the far field, which clips the field emitted with a divergence larger than 8 mrad. We examined the harmonic field divergence of the two satellites and saw that most of their harmonic components in the studied spectral range are emitted with divergences larger than 10 mrad therefore do not reach the far–field. The SAP FWHM in the far–field is 700 attoseconds, **longer than the pulse duration estimated in the near-field, because the trailing part of the far-field SAP is delayed. We examined its radial structure and observed that radiation arriving in the far-field off-axis is moved to slightly later times, i.e. the radiation has longer optical path to the periphery than along the optical axis causing**

the delay. ~~The length of the produced pulse is limited by the inherent atto chirp of the generation process.~~ We note that for the longer generating wavelength, the spread of return times is also larger. This is not a world record in single attosecond pulse duration, but this is also not the main advantage of the proposed arangement. We consider the main feature of this scheme the production of isolated attosecond burst from HHG performed with two long laser pulses, each of 50 fs duration.

We also investigated the stability of the SAP generation with respect to a very sensitive parameter which is the MIR pulse energy, exposed to shot-to-shot fluctuations in the experiments. We performed additional simulations with +/- 10% MIR pulse energy, while keeping the NIR pulse energy unchanged at 0.25 mJ. The first natural result was the shift of the cutoff, therefore we have also set a new spectral window for the attosecond pulse generation to be now 150-166 eV in order to include all three cases. The results show that primarily the SAP structure is preserved, both in near- and in far-field. Also the durations of the SAPs are similar, 300 attosec in the near-field. However, the best efficiency of SAP generation is found to be with the parameters discussed in the paper. With +10% pulse energy the satellites became more pronounced, thus reducing the intensity of the central SAP. Further increasing the MIR pulse energy leads to double attosecond pulse. With -10% MIR pulse energy the cutoff is lower, therefore the spectral filter catches less radiation, again leading to decreased SAP efficiency.

IV. Conclusion

In this paper we explored a HHG case which shows the potentials of strong mid-infrared pulses in order to obtain high photon flux up to 160 eV. In our configuration the strong MIR pulse is assisted by a weaker NIR pulse, a case which was not investigated before and is a novel alternative to the well–known two–color HHG.

In summary, we have shown that in HHG by a strong 1300 nm and a relatively weak 800 nm field: (a) At single–dipole level the periodicity of the successive emissions is increased to 1.5 o.c. of the MIR pulse, this means harmonic bursts once every 6.5 fs. (b) Even such a weak NIR presence ($1{\cdot}10^{14}$ W/cm^2 peak intensity in focus, but being before focus at -10 mm, the NIR never goes beyond $0.6{\cdot}10^{14}$ W/cm^2) changes the ionization dynamics within the combined pulse, causing serious intensity decrease for the primary MIR field shortly after the entrance in the medium, thus reducing the cutoff. (c) An almost constant "working intensity" is set in the second half of the long, high-pressure gas cell both along the propagation axis (z) and radially up to 40 μm, creating therefore a domain where the intensity gradient is small, this being a necessary condition for efficient, phase-matched HHG, increasing the overall harmonic yield by an order of magnitude compared to the MIR-only case.

We also demonstrated that there is a great possibility to obtain a SAP from the cutoff region in this MIR (strong) + NIR (weak) arrangement. The biggest advantage of the presented configuration is that the SAP has been obtained by using two laser pulses of 50 fs duration each, in parallel polarization.

The main message of this study is that exploring experimentally feasible generating conditions, it is possible to obtain strong XUV radiation up to 160 eV by two-color HHG, and even SAP can be obtained from 50 fs pulse with parallel polarization by filtering the cutoff domain (150–160 eV). The duration of the predicted SAP is ≈700 attoseconds ~~, mainly due to the relatively narrow spectral width of 10 eV~~ **because of the inherent atto chirp of the generation process and the enlarged trailing edge of the pulse in the far-field.**. However, it is centered at 155 eV, making it useful in pump–probe experiments requiring high-energy photons which can deepen our knowledge about the electron dynamics in molecules and solids at its natural time–scale.

Acknowledgment

We acknowledge the group in MBI Berlin lead by A. Rouzée and M.J.J. Vrakking for the useful discussions about the feasible experimental conditions. The authors KK and TV acknowledge support from projects PN–II–ID–PCE–2012–4–0342 and E02/2014 PULSE–PROPAG. MB, BE and VK acknowledge support from the Hungarian Scientific Research Fund (OTKA project NN107235).

References

[1] E. J. Takahashi, T. Kanai, K. L. Ishikawa, Y. Nabekawa, and K. Midorikawa, "Coherent water window x ray by phase-matched high-order harmonic generation in neutral media," *Phys. Rev. Lett.*, vol. 101, no. 25, p. 253901, 2008.

[2] B. E. Schmidt, A. D. Shiner, M. Giguère, P. Lassonde, C. A. Trallero-Herrero, J.-C. Kieffer, P. B. Corkum, D. M. Villeneuve, and F. Légaré, "High harmonic generation with long-wavelength few-cycle laser pulses," *J. Phys. B: At., Mol. Opt. Phys.*, vol. 45, no. 7, p. 074008, 2012.

[3] M.-C. Chen, C. Mancuso, C. Hernández-García, F. Dollar, B. Galloway, D. Popmintchev, P.-C. Huang, B. Walker, L. Plaja, A. A. Jaro-Becker, A. Becker, M. M. Murnane, H. C. Kapteyn, and T. Popmintchev, "Generation of bright isolated attosecond soft x-ray pulses driven by multicycle midinfrared lasers," *Proc. Natl. Acad. Sci. U.S.A.*, vol. 111, no. 23, pp. E2361–E2367, 2014.

[4] K.-H. Hong, C.-J. Lai, J. P. Siqueira, P. Krogen, J. Moses, C.-L. Chang, G. J. Stein, L. E. Zapata, and F. X. Kärtner, "Multi-mj, khz, 2.1 μm optical parametric chirped-pulse amplifier and high-flux soft x-ray high-harmonic generation," *Opt. Lett.*, vol. 39, no. 11, pp. 3145–3148, 2014.

[5] J. Tate, T. Auguste, H. G. Muller, P. Salières, P. Agostini, and L. F. DiMauro, "Scaling of wave-packet dynamics in an intense midinfrared field," *Phys. Rev. Lett.*, vol. 98, no. 1, p. 013901, 2007.

[6] A. D. Shiner, C. Trallero-Herrero, N. Kajumba, H.-C. Bandulet, D. Comtois, F. Légaré, M. Giguère, J.-C. Kieffer, P. B. Corkum, and D. M. Villeneuve, "Wavelength scaling of high harmonic generation efficiency," *Phys. Rev. Lett.*, vol. 103, no. 7, p. 073902, 2009.

[7] P. Rudawski, C. M. Heyl, F. Brizuela, J. Schwenke, A. Persson, E. Mansten, R. Rakowski, L. Rading, F. Campi, B. Kim, P. Johnsson, and A. L'Huillier, "A high-flux high-order harmonic source," *Rev. Sci. Instrum.*, vol. 84, no. 7, p. 073103, 2013.

[8] E. J. Takahashi, P. Lan, O. D. Muecke, Y. Nabekawa, and K. Midorikawa, "Attosecond nonlinear optics using gigawatt-scale isolated attosecond pulses," *Nat. Commun.*, vol. 4, p. 2691, 2013.

[9] J. F. Hergott, M. Kovacev, H. Merdji, C. Hubert, Y. Mairesse, E. Jean, P. Breger, P. Agostini, B. Carré, and P. Salières, "Extreme-ultraviolet high-order harmonic pulses in the microjoule range,"*Phys. Rev. A: At., Mol., Opt. Phys.*, vol. 66, p. 021801(R), 2002.

[10] K. Midorikawa, Y. Nabekawa, A. Suda, "XUV multiphoton processes with intense high-order harmonics", *Prog. Quant. Electr.*, vol. 32, pp. 43-88, 2008.

[11] P. Tzallas, E. Skantzakis, L. A. A. Nikolopoulos, G. D. Tsakiris, and D. Charalambidis, "Extreme-ultraviolet pumpprobe studies of one-femtosecond-scale electron dynamics", *Nature Physics*, vol. 7, pp. 781-784, 2011.

[12] W. Boutu, T. Auguste, O. Boyko, I. Sola, P. Balcou, L. Binazon, O. Gobert, H. Merdji, C. Valentin, E. Constant, E. Mével, and B. Carré, "High-order-harmonic generation in gas with a flat-top laser beam," *Phys. Rev. A: At., Mol., Opt. Phys.*, vol. 84, no. 6, p. 063406, 2011.
[13] J. Seres, V. Yakovlev, E. Seres, C. Streli, P. Wobrauschek, C. Spielmann, and F. Krausz, "Coherent superposition of laser-driven soft-x-ray harmonics from successive sources," *Nature Phys.*, vol. 3, no. 12, pp. 878–883, 2007.
[14] E. A. Gibson, A. Paul, N. Wagner, R. Tobey, D. Gaudiosi, S. Backus, I. P. Christov, A. Aquila, E. M. Gullikson, D. T. Attwood, M. M. Murnane, and H. C. Kapteyn, "Coherent soft x-ray generation in the water window with quasi-phase matching," *Science*, vol. 302, no. 5642, pp. 95–98, 2003.
[15] K. Cassou, S. Daboussi, O. Hort, O. Guilbaud, D. Descamps, S. Petit, E. Mével, E. Constant, and S. Kazamias, "Enhanced high harmonic generation driven by high-intensity laser in argon gas-filled hollow core waveguide," *Opt. Lett.*, vol. 39, no. 13, pp. 3770–3773, 2014.
[16] A. Paul, R. Bartels, R. Tobey, H. Green, S. Weiman, I. Christov, M. Murnane, H. Kapteyn, and S. Backus, "Quasi-phase-matched generation of coherent extreme-ultraviolet light," *Nature*, vol. 421, no. 6918, pp. 51–54, 2003.
[17] K. Kovács, E. Balogh, J. Hebling, V. Toşa, and K. Varjú, "Quasi-phase-matching high-harmonic radiation using chirped thz pulses," *Phys. Rev. Lett.*, vol. 108, no. 19, p. 193903, 2012.
[18] S. L. Voronov, I. Kohl, J. B. Madsen, J. Simmons, N. Terry, J. Titensor, Q. Wang, and J. Peatross, "Control of laser high-harmonic generation with counterpropagating light," *Phys. Rev. Lett.*, vol. 87, no. 13, p. 133902, 2001.
[19] X. Zhang, A.L Lytle, T. Popmintchev,X. Zhou,H.C. Kapteyn, M.M. Murnane, O. Cohen, "Quasi-phase-matching and quantum-path control of high-harmonic generation using counterpropagating light," *Nature Physics*, vol. 3, no. 4, p. 270–275, 2007.
[20] A. Heinrich, W. Kornelis, M. P. Anscombe, C. P. Hauri, P. Schlup, J. Biegert, and U. Keller, "Enhanced vuv-assisted high harmonic generation," *J. Phys. B: At., Mol. Opt. Phys.*, vol. 39, no. 13, p. S275, 2006.
[21] J. Biegert, A. Heinrich, C. Hauri, W. Kornelis, P. Schlup, M. Anscombe, K. Schafer, M. Gaarde, and U. Keller, "Enhancement of high-order harmonic emission using attosecond pulse trains," *Laser Phys.*, vol. 15, no. 6, pp. 899–902, 2005.
[22] B. A. Reagan, T. Popmintchev, M. E. Grisham, D. M. Gaudiosi, M. Berrill, O. Cohen, B. C. Walker, M. M. Murnane, J. J. Rocca, and H. C. Kapteyn, "Enhanced high-order harmonic generation from xe, kr, and ar in a capillary discharge," *Phys. Rev. A: At., Mol., Opt. Phys.*, vol. 76, no. 1, p. 013816, 2007.
[23] J. A. Pérez-Hernández, D. J. Hoffmann, A. Zaïr, L. E. Chipperfield, L. Plaja, C. Ruiz, J. P. Marangos, and L. Roso, "Extension of the cut-off in high-harmonic generation using two delayed pulses of the same colour," *J. Phys. B: At., Mol. Opt. Phys.*, vol. 42, no. 13, p. 134004, 2009.
[24] E. Cormier and M. Lewenstein, "Optimizing the efficiency in high order harmonic generation optimization by two-color fields," *Eur. Phys. J. D*, vol. 12, no. 2, pp. 227–233, 2000.
[25] I. J. Kim, C. M. Kim, H. T. Kim, G. H. Lee, Y. S. Lee, J. Y. Park, D. J. Cho, and C. H. Nam, "Highly efficient high-harmonic generation in an orthogonally polarized two-color laser field," *Phys. Rev. Lett.*, vol. 94, no. 24, p. 243901, 2005.
[26] H. Mashiko, S. Gilbertson, C. Li, E. Moon, and Z. Chang, "Optimizing the photon flux of double optical gated high-order harmonic spectra," *Phys. Rev. A: At., Mol., Opt. Phys.*, vol. 77, no. 6, p. 063423, 2008.
[27] C. Vozzi, F. Calegari, F. Frassetto, L. Poletto, G. Sansone, P. Villoresi, M. Nisoli, S. De Silvestri, and S. Stagira, "Coherent continuum generation above 100 ev driven by an ir parametric source in a two-color scheme," *Phys. Rev. A: At., Mol., Opt. Phys.*, vol. 79, no. 3, p. 033842, 2009.
[28] L. Brugnera, F. Frank, D. J. Hoffmann, R. Torres, T. Siegel, J. G. Underwood, E. Springate, C. Froud, E. I. C. Turcu, J. W. G. Tisch, and J. P. Marangos, "Enhancement of high harmonics generated by field steering of electrons in a two-color orthogonally polarized laser field," *Opt. Lett.*, vol. 35, no. 23, pp. 3994–3996, 2010.
[29] E. J. Takahashi, P. Lan, O. D. Mücke, Y. Nabekawa, and K. Midorikawa, "Infrared two-color multicycle laser field synthesis for generating an intense attosecond pulse," *Phys. Rev. Lett.*, vol. 104, no. 23, p. 233901, 2010.
[30] J. Luo, W. Hong, Q. Zhang, K. Liu, and P. Lu, "Dramatic cutoff extension and broadband supercontinuum generation in multi-cycle two color pulses," *Opt. Express*, vol. 20, no. 9, pp. 9801–9809, 2012.
[31] E. Priori, G. Cerullo, M. Nisoli, S. Stagira, S. De Silvestri, P. Villoresi, L. Poletto, P. Ceccherini, C. Altucci, R. Bruzzese, and C. de Lisio, "Nonadiabatic three-dimensional model of high-order harmonic generation in the few-optical-cycle regime," *Phys. Rev. A: At., Mol., Opt. Phys.*, vol. 61, no. 6, p. 063801, 2000.
[32] V. Tosa, C. Altucci, K. Kovacs, M. Negro, S. Stagira, C. Vozzi, and C. Velotta, "Isolated attosecond pulse generation by two-mid-ir laser fields," *IEEE J. Sel. Topics Quantum Electron.*, vol. 18, no. 1, pp. 239–247, 2012.
[33] M. Lewenstein, P. Salières, and A. L'Huillier, "Phase of the atomic polarization in high-order harmonic generation," *Phys. Rev. A: At., Mol., Opt. Phys.*, vol. 52, no. 6, pp. 4747–4754, 1995.
[34] K. Kovács and V. Toşa, "Quantum trajectories of electrons in arbitrary laser fields," *J. Mod. Opt.*, vol. 57, no. 11, pp. 977–983, 2010.
[35] V. Tosa, E. Balogh, and K. Kovács, "Phase-matched generation of water-window x rays," *Phys. Rev. A: At., Mol., Opt. Phys.*, vol. 80, no. 4, p. 045801, 2009.
[36] B. Schütte, P. Weber, K. Kovács, E. Balogh, B. Major, V. Tosa, S. Han, M. J. J. Vrakking, K. Varjú, and A. Rouzée, "Bright attosecond soft x-ray bursts by transient phase-matching in two-color high-order harmonic generation," in preparation.
[37] T. Popmintchev, M. C. Chen, A. Bahabad, M. Gerrity, P. Sidorenko, O. Cohen, I. P. Christov, M. M. Murnane, and H. C. Kapteyn, "Phase matching of high harmonic generation in the soft and hard X–ray regions of the spectrum," *Proc. Natl. Acad. Sci. U.S.A.*, vol. 106, no. 26, pp. 10516–10521, 2009

Katalin Kovács was born in Odorheiu Scuiesc, Romania, in 1980. She received the B.S. degree in Physics, in 2002, and the PhD degree in 2007, in the field of modeling and simulation of magnetization phenomena with statistical physics methods from the Faculty of Physics of Babeş–Bolyai University at Cluj-Napoca, Romania. Since 2007, she has been a Researcher at the National Institute for R&D in Isotopic and Molecular Technologies,Cluj-Napoca, Romania. Her current research interests are focused on modeling HHG and attosecond pulse formation in the interaction of ultrashort laser pulses with gaseous media.

Balázs Major was born in Szeged, Hungary, in 1988. He received his Bachelor's degree in 2010, and his Master's degree in Physics in 2012 from Uinversity of Szeged, Hungary. He is currently a PhD student at the Department of Optics and Quantum Electronics of University of Szeged. As an undergraduate he was interested in photoluminescence measurements of industrial silicon samples and later femtosecond pulse focusing. His current research topics include theoretical and experimental investigations on focusing and diffraction of ultrashort optical pulses, high-harmonic generation and scattering of fractal-like aerosol aggregates.

Emeric Balogh was born in 1985 in Salonta, Romania. He received his Bachelor's degree in Physics and Computer Science in 2008 and his Master's degree in Physics in 2010 from the Babes-Bolyai University, Cluj-Napoca, Romania. During his studies he has researched correlations in stock-markets and modeled virus spreading in biological cell cultures. Since 2010 he is a PhD student at the University of Szeged, Hungary. Hes research interest includes high-order harmonic– and attosecond pulse generation by MIR and two-color pulses, and quasi-phase-matching.

Valer Toşa was born in Bedeciu, Romania, in 1955. He received the B.S. degree from the Physics Faculty of Babes-Bolyai University in Cluj-Napoca, Romania, in 1979, with a thesis on energy band calculations, and was awarded the PhD degree in 1992, for the work done on multiphoton excitation and vibration relaxation of polyatomic molecules. Since 1982, he is a researcher with the National Institute for R&D in Isotopic and Molecular Technologies, Cluj-Napoca, Romania, working presently as Principal Investigator. His research interests are in computer modeling of laser interaction with atoms and molecules (multiphoton processes, high-order harmonic generation). He also works in computer modeling of substance migration in multilayer packaging systems. Dr. Tosa is a member of the Romanian Physical Society and SPIE.

Katalin Varjú graduated with an MSc in Physics with Distinction in 1999 at the JATE University of Szeged, Hungary. She carried out postgraduate studies jointly at the University of Kent at Canterbury (UK) and the University of Szeged in the field of General relativistic effects on quantum spin-1/2 particles, and received a PhD award with Distinction in 2002. As a postdoc she started working on a high-power laser system at the Department of Optics and Quantum Electronics at the University of Szeged. Supported by the EU's Marie Curie programme she spent two and a half years at Lund University in the group of Anne L'Huillier, where she started studying high–order harmonic– and attosecond pulse generation, characterization and application. At present she is leading an attosecond research group at the University of Szeged. She is also involved in designing one of the beamlines of the ELI ALPS infrastructure.